Dalton Transactions

Hydrogen Isotope Separation at Exceptional High Temperature Using Unsaturated Organometallic Complex

Journal:	*Dalton Transactions*
Manuscript ID	DT-ART-10-2024-003018.R1
Article Type:	Paper
Date Submitted by the Author:	18-Dec-2024
Complete List of Authors:	Kitayama, Taku; Tohoku University Yamauchi, Tamon; Tohoku University Uchida, Kaiji; Tohoku University Tanaka, Shunya; Tohoku University Toyoda, Ryojun; Tohoku University Iguchi, Hiroaki; Tohoku University Sakamoto, Ryota; Tohoku University Xue, Hao; Tohoku University Kishimoto, Naoki; Tohoku University Yoshida, Takefumi; Wakayama University Uruga, Tomoya; SPring-8 Noro, Shin-ichiro; Hokkaido University Takaishi, Shinya; Tohoku University

ARTICLE

Hydrogen Isotope Separation at Exceptional High Temperature Using Unsaturated Organometallic Complex

Received 00th January 20xx,
Accepted 00th January 20xx

DOI: 10.1039/x0xx00000x

Taku Kitayama,[a] Tamon Yamauchi,[a] Kaiji Uchida,[a,b] Shunya Tanaka,[a] Ryojun Toyoda,[a] Hiroaki Iguchi,[a] Ryota Sakamoto,[a] Hao Xue, [a] Naoki Kishimoto, [a] Takefumi Yoshida,[c] Tomoya Uruga,[d,e] Shin-ichiro Noro,[f] and Shinya Takaishi*[a,g]

A new approach for hydrogen isotope separation using an unsaturated organometallic complex was proposed. Adsorption measurements of $[Mn(dppe)_2(CO)(N_2)](BArF^{24})$ (**Mn-dppe**) (dppe = 1,2-bis(diphenylphosphino)ethane, $BArF^{24}$ = $B[C_6H_3(3,5\text{-}CF_3)_2]_4$) using H_2 and D_2 revealed a significant difference in the adsorption enthalpy of H_2/D_2 at much higher room temperatures than in previous studies, with D_2 molecules being more strongly adsorbed on unsaturated metal sites. Mixed gas adsorption isotherms were calculated at each temperature using IAST theory, and it was predicted that D_2 uptake was much larger than H_2 uptake. Column chromatographic separation using the difference in adsorption enthalpy indicated that deuterium could be concentrated, and DFT calculations suggest that this difference in adsorption force is due to the difference in vibrational potentials involved in metal-dihydrogen bonding. This study introduces a new separation approach that could enable hydrogen isotope separation in the ambient temperature range.

Introduction

Deuterium (D) and tritium (T), isotopes of hydrogen, have many applications in science, medicine, and industry, such as heavy water nuclear reactors,[1] neutron scattering technology[2], drug discovery and development,[3] nuclear magnetic resonance spectroscopy[4] and isotope tracing.[5] Due to its significance in industry and scientific research, D_2 has become an irreplaceable element. Despite the demand, deuterium accounts for only 0.015% of naturally occurring hydrogen, and a simple and energy-saving process for producing deuterium has not yet been established because the two isotopes have almost identical size, shape, and thermodynamic properties. Thus, industrial hydrogen isotope separation methods currently in use, such as cryogenic distillation or electrolysis of heavy water produced by the Girdler sulfide process, are time- and energy-intensive and have low selectivity. As energy conservation is advocated toward a carbon-neutral society, alternative methods to these energy comsumptive methods are required.

Quantum sieving is one of the direct methods for hydrogen isotope separation. Kinetic quantum sieves (KQS) describes the effect of lighter isotopes with larger deBroglie wavelengths encountering higher energy barriers as they diffuse through fine pores at cryogenic temperatures and several KQS have been reported.[6-8] However, it is challenging to strike a balance between selectivity and adsorption capacity since the pore size restriction increase the selectivity of gas separation ,while it decreases adsorption capacity. Furthermore, low-temperature separation conditions require much energy. Recently, chemical affinity quantum sieves (CAQS) using MOFs with open metal site attract attention as separating materials for hydrogen isotopes. The CAQS effect is used to separate hydrogen isotopes through thermodynamic effects. FitzGerald et al. first studied the CAQS effect at the strong adsorption site in MOF 74 (M = Fe, Co, Ni)

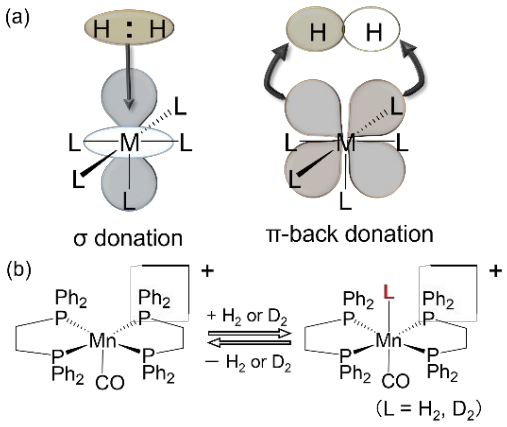

Fig. 1 (a)Kubas interaction (b)H_2/D_2 adsorption on $[Mn(CO)(dppe)_2](BArF^{24})$.

[a] Department of Chemistry, Graduate School of Science, Tohoku University, 6-3 Arama-ki-Aza-Aoba, Aoba-ku, Sendai 980-8578, Japan.
[b] Tokyo Metropolitan Industrial Technology Research Institute, 2-4-10 Aomi, Koto, Tokyo 135-0064, Japan.
[c] Cluster of Nanomaterials, Graduate School of Systems Engineering, Wakayama University. 930 Sakaedani, Wakayama, 640-8510, Japan.
[d] Research & Utilization Division, Japan Synchrotron Radiation Research Institute, SPring-8, Sayo, Hyogo 679-5198, Japan
[e] Innovation Research Center for Fuel Cells, The University of Electro-Communications, Chofu, Tokyo, 182-8585 Japan
[f] Faculty of Environmental Earth Science, Hokkaido University, Sapporo 060-0810, Japan
[g] Physical and Chemical Research Infrastructure Group, RIKEN SPring-8 Center, RIKEN, Sayo, Hyogo, Japan E-mail: shinya.takaishi.d8@tohoku.ac.jp

† Electronic Supplementary Information (ESI) available: Experimental details, adsorption isotherm, breakthrough experiment, structural models used for DFT calculations. See DOI: 10.1039/x0xx00000x

Table 1 Thermodynamic parameters of Mn-dppe calculated by van't Hoff equation and averaged Qst value calculated by isosteric heat analysis

	H_2	D_2	R^2 value (van't Hoff plot)	Q_{st}_ave. / kJ·mol^{-1}	R^2 value (isosteric heat of adsorption analysis)
ΔS / J·mol^{-1}·K^{-1}	–121.7(18)	–129.3(13)	0.9994	–49.2	0.9944
ΔH / kJ·mol^{-1}	–50.2 (6)	–54.4 (4)	0.9997	–53.9	0.9983

in 2013.[9] In recent years, many examples of hydrogen isotope separation by MOFs using CAQS effect have been reported.[10-12]

However, among the vast library of the hydrogen isotope separating materials, no example show hydrogen isotope separation ability with ambient temperature, due to their low adsorption enthalpy. In addition, its difficulty to synthesize MOFs with unsaturated metal sites lowered designability and prevented development of these types of materials.[13-16] Hence, to address this issue, hydrogen adsorbing materials with higher hydrogen adsorption enthalpy should be utilized to increase working temperature, and simple structural materials should be adopted.

Unsaturated organometallic complexes have high enthalpies of adsorption; Abrecht et al. investigated the H_2 adsorption on the vacancy sites created by the desorption of nitrogen upon activation of [Mn(dppe)$_2$(CO)(N$_2$)](BArF^{24}) (**Mn-dppe**) (dppe = 1,2-bis(diphenylphosphino)ethane, BArF^{24} = B[C$_6$H$_3$(3,5-CF$_3$)$_2$]$_4$).[17] The dihydrogen complex can reversibly adsorb and desorb dihydrogen in the solid state despite the fact that it is a discrete complex with no porosity, and its enthalpy of hydrogen adsorption is –52.2 kJ/mol. In our previous study, we also reported that dinitrogen complexes can be used to desorb nitrogen in the solid state and reversibly adsorb molecular hydrogen to unsaturated metal sites, with hydrogen adsorption enthalpies of –47.3 kJ/mol.[18, 19] These high enthalpy to adsorb H_2 were due to their strong and specific interaction between metal and H_2. based on σ donation and π-back donation (Fig. 1(a)). In addition, isotope effect on dihydrogen complex in solution was confirmed theoritically and experimentally.[20] Thus, these experimental results suggest that discrete dihydrogen complexes are not only hydrogen adsorbents with high enthalpies of adsorption, but also have potential applications in high temperature isotope separation (Fig 1(b)).

Herein, we present a novel approach using a simple unsaturated organometallic complex as hydrogen isotope separating material. ; [Mn(dppe)$_2$(CO)][BArF^{24}]. The complex exhibits the high selectivity of 1.9 for D_2 over H_2 at exceptional high temperature even over 300 K.

Result and Discussion

H_2/D_2 sorption measurement

Mn-dppe was synthesized by modified procedure. Detail is described in supporting information. This complex has vacant metal site and hydrogen molecule can adsorb directly to metal. Ad/desorption measurement was carried out from 313 K to 363 K.

Adsorption isotherm showed Langmuir adsorption behavior.(Fig. 2(a) (b)) and H_2 and D_2 adsorbed reversibly. All isothems were well reproduced by the langmuir equations as follows,

$$\frac{V}{V_{max}} = \frac{Kp}{1 + Kp} \quad (1)$$

where V, V_{max}, K and p represent the volume of adsorbate, saturated adsorption capacity of adsorbent, adsorption equilibrium constant and gas pressure, respectively. We fitted the isotherms with two parameters, K and V_{max}, in which V_{max} was commonly refined using all data by the global fitting, whereas K was refined for each temperature. We obtained each V_{max} value of 12.42 cm^3(STP) g^{-1} and 12.44 cm^3(STP) g^{-1} for H_2 and D_2 adsorption, respectively (Table S1). Assuming one H_2 or D_2 molecule bound to one Mn(I) site, the estimated V_{max} value was 12.86 cm^3(STP) g^{-1}. Thus, we estimated that 97% of Mn(I) sites were used, indicating that almost all of the Mn(I) open-metal sites were accessible in spite of the non-porous structure.

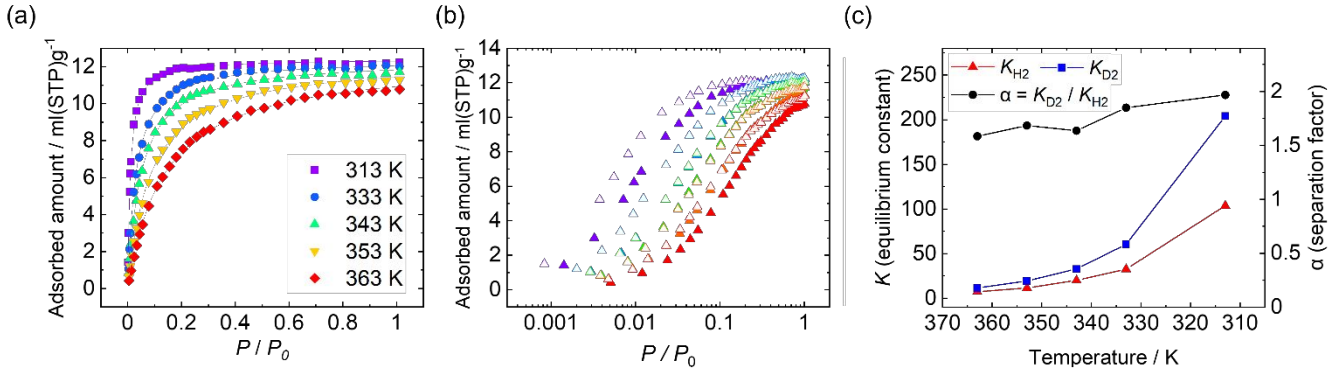

Fig. 2 (a) H_2 adsorption isotherm for **Mn-dppe** (b)Comparison of H_2 and D_2 adsorption isotherm for **Mn-dppe;** filled triangle and open triangle represent H_2 isotherm and D_2 isotherm, and red, orange, green, blue, purple points represent 363K, 353K, 343K, 333K, 313K respectively. (c)plot of separation factor and equilibrium constant for **Mn-dppe** against temperature

Table 2 selectivity of D_2 over H_2 of **Mn-dppe** calculated from pure gas adsorption isotherm using IAST theory

P_{total} / kPa	0.1	1	10	20	30	40	50	60	70	80	90	100
S (313K)	1.98	1.98	1.97	1.97	1.97	1.97	1.97	1.97	1.96	1.96	1.96	1.962
S (333 K)	1.83	1.83	1.84	1.84	1.85	1.85	1.85	1.85	1.85	1.85	1.85	1.851
S (343 K)	1.59	1.59	1.60	1.61	1.61	1.61	1.62	1.62	1.62	1.62	1.62	1.624
S (353 K)	1.67	1.67	1.67	1.67	1.68	1.68	1.68	1.68	1.68	1.68	1.68	1.680
S (363 K)	1.68	1.67	1.66	1.65	1.65	1.64	1.64	1.63	1.63	1.63	1.62	1.621

This quantitative adsorption could be attributed to dynamic porosity[21].

We measured the in-situ X-ray absorption fine structure (XAFS) at the Mn K-edge to estimate the structural and electronic changes before and after H_2 adsorption. The in-situ XAFS revealed a clear disappearance of the pre-edge peak at 6532 eV (Fig. S4(b)) following H_2 adsorption. This pre-edge peak corresponds to the Laporte-forbidden 1s→3d transition, which is partially allowed in non-centrosymmetric complexes. Therefore, this phenomenon can be reasonably explained by a geometrical change from a non-centrosymmetric, five-coordinated state to a pseudo-centrosymmetric, six-coordinated state. Additionally, the white-line intensity increased in the H_2-adsorbed complex. This transition corresponds to the 1s→4p transition. The increase in white-line intensity suggests that the H_2-adsorbed complex possesses higher symmetry, leading to a greater degeneracy of the 4p orbitals. In contrast, the EXAFS region showed small difference before and after H_2 adsorption (Fig. S4(c) and (d)), but neither the Mn-P nor Mn-C bonds exhibited significant changes (Table S2), suggesting that there was no major alteration in the phosphine and carbonyl ligands as a result of H_2 adsorption.

The thermodynamic parameters were evaluated using van't Hoff equation as follows,

$$\ln K = -\frac{\Delta H}{RT} + \frac{\Delta S}{R} \quad (2)$$

where $\Delta H°$ is the standard molar enthalpy change of adsorption, $\Delta S°$ is the standard molar entropy change of adsorption and R is the ideal gas constant. Enthalpy change of H_2 adsorption ($\Delta H°_{H2}$) was −50.2 kJ/mol, while the that of D_2 adsorption ($\Delta H°_{D2}$) was −54.4 kJ/mol. These values are reasonable from the isosteric heat of adsorption analysis (Table 1 and Fig. S3). H_2 and D_2 were adsorbed on **Mn-dppe** even at ambient temperature or higher (313 K – 363 K) due to these high adsorption enthalpy. The difference of the adsorption enthalpy between H_2 and D_2 was 4.2 kJ/mol when calculated with van't Hoff equation and 4.7 kJ/mol when calculated by isosteric heat analysis. These values are significantly higher than that of MFU-4l (2.3-2.4 kJ/mol), known as high temperature CAQS.[22] Separation factor, which could be calculated from equilibrium constant for gas adsorption of each hydrogen isotope, was 1.9 even at ambient temperature (313 K). This result indicated hydrogen isotope separation at ambient temperature could be realized.

Mixed gas adsorption analysis by IAST method

While pure gas sorption measurement gave the difference between H_2 and D_2, they do not express actual selectivity that would be obtained with a gas mixture. Although mixed gas sorption measurement were necessary, it requires difficult technique and specific instrument. Then, mixed gas adsorption isotherms were calculated from single component adsorption isotherms using idealized adsorption solution theory (IAST).[23-25] This method is often applied to quantum sieves including CAQS. Predicted mixed gas adsorption data was described in Fig. S6. The data clearly showed the enhanced adsorption of D_2 over H_2. The selectivity is defined as the ratio of molar fractions in the adsorbed phase (x) and gas phase (y),

$$S = \frac{x_{D_2}/y_{D_2}}{x_{H_2}/y_{H_2}} \quad (3)$$

The calculated selectivity was described in the Table 2 and Fig. S7. Selectivity was correlated with the differences in equibrium constants between H_2 and D_2, and thus, the highest selectivity was 1.98 at 313 K (P_{total} = 0.1 bar). Selectivity and working temperature was compared with other CAQS at high working temperature (Fig. S8 and Table S3). Working temperature of **Mn-dppe** was the highest of the other isotope separating materials for now.

Breakthrough measurement

Next, breakthrough experiment of the hydrogen isotope was conducted to investigate the separation ability of the mixed gas. A 6.0 mmφ glass column was filled with 1.0 g of **Mn-dppe** and

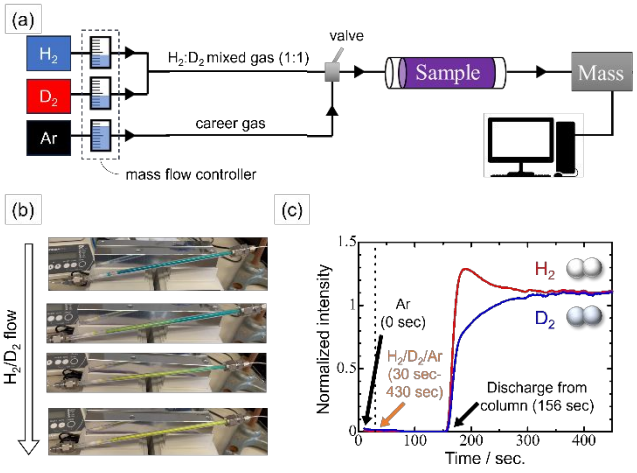

Fig. 3 (a) Setup for H_2/D_2 mixed gas breakthrough measurement (b) Change over time during breakthrough measurement (c) Detected volume of gas emitted versus time (normalized from blank measurement results); red line represented the amount of H_2 and blue point represented the one of D_2

Ar was the carrier gas, H_2/D_2 mixed gas (H_2: 3.0 ml·min^{-1}, D_2: 3.0 ml·min^{-1}, Ar: 6.0 ml·min^{-1}, total pressure: 1 bar) flowed into the column at 80 °C from 30 seconds to 430 seconds after the start of measurement, and the gases from the column were detected by mass spectrometer (Fig. 3(a)). In the course of the experiment, the colour of the powder changed from emerald-green to yellow, which indicated **Mn-dppe** changed into **Mn-dppe**-H_2 by dihydrogen adsorption (Fig. 3(b)). The breakthrough curve was shown in Fig. 3(c). 126 seconds after gas flow started, the gas started to flow out of column and the amount of H_2 was clearly larger than D_2 for about 50 second, because H_2 and D_2 competitively adsorbed on the unsaturated metal site and D_2 coordinated more strongly due to the larger adsorption equilibrium constant at the same temperature. The result showed the concentration of H_2 from mixed gases could be possible. Hence, we first demonstrated the possibility of the hydrogen isotope separation at ambient condition, using column chromatography filled with unsaturated complex. However, HD was also detected, albeit in smaller quantities, indicating that an H/D exchange reaction had also occurred.[26] The generation of HD was attributed to the high working temperature (80 °C) required to desorb H_2 and D_2 from the metal. Therefore, smaller $\Delta H°$ which allows the lowering operating temperature should be important to avoid the H/D exchange reaction.

DFT calculation

DFT calculations were conducted for several Mn complexes including Mn-dppe to explain the high separation value of the complex. For the calculation, Mn-dppe$^+$ (cationic part of Mn-dppe) and Mn-dppe$^+$-H_2 (H_2 adducts on Mn-dppe) was adopted, and several kinds of functions were utilized. First, we estimated the thermodynamic parameters of H_2 and D_2 adsorption. The adsorption thermodynamic parameters were calculated as follows;

$$\Delta H^{\circ}_{\mathrm{ads}} = H^{\circ}(\textbf{Mn-dppe}^{+}\text{-}H_2) - H^{\circ}(\textbf{Mn-dppe}^{+}) - H^{\circ}(H_2)$$

where H° represent standard molar enthalpy.

The calculated adsorption enthalpies of H_2/D_2 and the difference between H_2 and D_2 were listed on Table S4. Although the absolute value of the adsorption enthalpies was different by the used function, the difference of adsorption enthalpy between H_2 and D_2 adsorption ($\Delta\Delta H^{\circ}$) were consistent with experimental results, which indicated that calculations can be used to discuss the magnitude of isotope effect. The difference of total vibration energy between **Mn-dppe**$^+$-H_2 and **Mn-dppe**$^+$-D_2 was 12.51 kJ/mol though that between H_2 and D_2 was 7.73 kJ/mol, which indicated M-H_2 bonding enhance isotope effect remarkably. This difference was assigned as the sum of the vibrational difference involved with dihydrogen. Especially, the sum of the difference of the three vibration modes ($\Delta\nu_{\mathrm{sym}}$ + $\Delta\nu_{\mathrm{asym}}$ + $\Delta\nu_{\mathrm{H-H}}$) was 10.89 kJ /mol, and account for about 87% of total vibrational energy, shown in Fig. 4. Thus, these three vibrational modes mainly contributed to the isotope effect between H_2/D_2. Next, we calculated several models of unsaturated complexes along with their H_2 and D_2 adducts (Fig. S11-13 and **Table. S6-S23**). The values of $\Delta\nu_{\mathrm{sym}}$, $\Delta\nu_{\mathrm{asym}}$,and $\Delta\nu_{\mathrm{H-H}}$ were proportional to those of ν_{sym}, ν_{asym}, and $\nu_{\mathrm{H-H}}$ for H_2 and D_2 adducts, indicating that the higher frequencies in these three vibrational modes brings about the greater frequency differences between H_2 and D_2 adducts (Fig. S9). Therefore, complexes with higher frequencies in the three vibrational modes are promising. In other words, it is important to design complexes with strong M-H_2 bonding without weakening the H-H bond, which often presents a trade-off because of the π-back donation from metal to H_2. To examine each vibration mode in detail, the correlation between the separation factor and the frequency of each vibration mode is shown in Fig. S10. $\Delta\nu_{\mathrm{sym}}$ and $\Delta\nu_{\mathrm{asym}}$ were positively correlated with the separation factor, respectively, while $\Delta\nu_{\mathrm{H-H}}$ showed no correlation. These correlations can be explained by the characteristics of the M-H_2 bonding in the cationic complexes, where the influence of the σ donation from H_2 to metal is dominant compared to π-back donation from metal to H_2.[17] In other words, strengthening the M-H_2 bonding in cationic complexes is crucial for increasing the separation factor.

Conclusions

In summary, a novel hydrogen isotope separation method to increase working temperature above room temperature was established, which showed the difference of adsorption enthalpy of hydrogen isotpe on the unsaturated organometallic complex; **Mn-dppe**. This method not only provides an effective way to separate hydrogen isotope via adsorption-desorption method, but also allows easier column chromatography separation under ambient condition. Computational methods clarified that the contribution of the vibrations involved with M-H_2 bond is very large. Experimental and computational results suggested a design guideline for highly isotope separation materials as follows, unsaturated complexes with moderate hydrogen adsorption enthalpy and high frequencies for three vibrational modes of ν_{sym}, ν_{asym}, and $\nu_{\mathrm{H-H}}$. Especially in cationic complexes, strengthening M-H_2 bonding is quite important to increase separation factor. These findings open a pathway to achieving energy-efficient hydrogen isotope separation as an alternative to cryogenic distillation.

Experimental

General synthetic procedure

All synthesis procedures were performed under anaerobic conditions using standard Schlenk-line techniques in a commercial glovebox under argon atmosphere. $Mn(CO)_5Br$ and other chemical reagent purchased from commercial sources were of reagent grade. The solvents were dried using common drying agents.

Preparation of trans-[Mn(dppe)$_2$(CO)Br]

This procedure was a modification of one in the literature,[17] synthesized with one-step reaction. $Mn(CO)_5Br$ (517 mg, 1.89 mmol) and dppe (1602 mg, 4.02 mmol) were dissolved in deoxidized toluene in a 100 ml round-bottom flask and allowed to stir for overnight under irradiation with UV light (365 nm), causing the precipitation of red-orange solid. UV irradiation continue until CO gas release stopped formed. The solid was filtered and washed with hexane. The compound was used for next reaction without further purification. Yield: 1363 mg (1.42 mmol ,74.8%)

Preparation of [Mn(dppe)$_2$(CO)](BArF) (Mn-dppe)

This compound was synthesized using an anion substitution process with a slight modification.[17,27] $[Mn(dppe)_2(CO)_3Br]$ (96 mg, 0.1 mmol) was dissolved in dichloromethane (−20 °C) in a 30 ml vial in the Ar glove box, dried Na[BArF^{24}] (89 mg, 0.1 mmol) were added to the solution, and then turned to dark green solution. The solution allowed to stir for 1 h, and filtered using celite to remove NaBr. The solvent was removed in vacuo, and dark green solid were remained. The solid was redissolved in a little dichloromethane and slow diffusion with hexane. After several days, dark green crystalline solid was formed and filtered. The compound was grinded before ad/desorption measurement. Yield: 68%. Elemental analysis (%) for $C_{85}H_{60}OP_4BF_{24}Mn$, calc.: C, 58.57; H, 3.47; Found: C, 58.28; H, 3.49. ^{1}H NMR (500 MHz) in C_6D_6 under argon atmosphere δ = 2.0 (d, 8H); δ = 6.1-8.5 (m, 52H). ^{31}P NMR (500 MHz) in C_6D_6: δ = 80.3 (s). ^{19}F NMR (500 MHz) in C_6D_6: δ = −62.0 (s).

Physical measurement

Measurements H_2 and D_2 sorption isotherm was performed using microtracbel Belsorp Max. IR spectra were recorded as KBr pellets on a JASCO FT/IR-4200 spectrometer at room temperature. For acquiring IR spectra under inert atmosphere, the KBr pellets were fabricated in glove box (MBRAUN UNILAB1200/780) filled with Ar gas, and then the pellets were set into a specially designed sealed optical cell individually. Elemental analyses were performed using J-Science Lab JM-10 equipped in the research and analytical center for giant molecules at Tohoku University. X-ray absorption fine structure (XAFS) measurement was conducted at the BL-36XU beamline in the Spring-8. The X-rays were monochromatized with a Si(111). Ground sample was placed in a silica glass capillary with an inner diameter 0.75 mm and the capillary was connected to stainless-steel lines with valves to dose and remove gas. The XAFS data was processed using the ATHENA program.

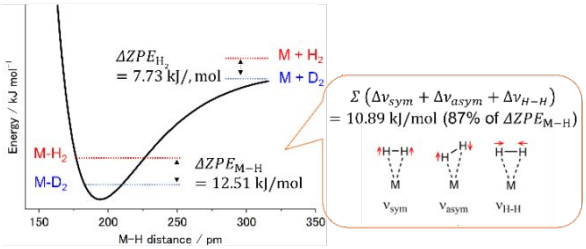

Fig. 4 Comparison of the energy diagram between H_2 and D_2 adducts and the typical vibration modes with the largest contribution to the difference

Computational analysis

DFT calculations were performed as implemented in the Gaussian 16 software. [28] Geometry optimization and frequency analysis were performed using B3LYP,[29] M06,[30] and wB97X-D[31] functional and def2-TZVP,[32] aug-cc-pVDZ,[33] and 6-31G[34] basis sets for Mn, H_2 or D_2, and others, respectively. Thermodynamic parameters were obtained by following procedure.

Geometry optimization and vibrational analysis were performed for the singlet spin state of coordinatively-unsaturated complexes $[Mn(dppe)_2(CO)]^+$, H_2- or D_2-adduct of each complexes $[Mn(\eta^2\text{-}H_2 \text{ or } \text{-}D_2)(dppe)_2(CO)]^+$ and free H_2 or D_2 molecule. For coordinatively-unsaturated complexes and H_2 or D_2 adducts, initial structure was derived from the crystal structure data[27,35]. Standard molar Gibbs free energy change (ΔG°_{ads}), standard molar enthalpy change (ΔH°_{ads}) and standard molar entropy change (ΔH°_{ads}) of adsorption were calculated by following equation,

$$\Delta H^\circ_{ads} = H^\circ(\mathbf{M-H_2}) - H^\circ(\mathbf{M}) - H^\circ(\mathbf{H_2})$$
$$\Delta G^\circ_{ads} = G^\circ(\mathbf{M-H_2}) - G^\circ(\mathbf{M}) - G^\circ(\mathbf{H_2})$$
$$\Delta S^\circ_{ads} = S^\circ(\mathbf{M-H_2}) - S^\circ(\mathbf{M}) - S^\circ(\mathbf{H_2})$$

where the subscript M-H_2, H_2 and M represent H_2-adduct, free H_2 molecule and 16-electron complex, respectively.

Author contributions

TK wrote paper together with TY., KU., RT, HI., RS. and ST. The synthesis and general measurements were performed by TK, TY, KU, ST. and ST. XAFS measurement were performed with TY and TU. Breakthrough measurement were performed with SN. Quantum chemical calculation was performed by KU, HX, and NK. S.T directed the project.

Conflicts of interest

There are no conflicts to declare.

Data availability

All data associated with this manuscript are available in the ESI.†

Acknowledgements

This work was supported by a JSPS KAKENHI Grant Nos. 23H02054, 21H04696, 19H02729, Adaptable and Seamless Technology transfer Program through Target-driven R&D (A-STEP) from Japan Science and Technology Agency (JST) Grant Number JPMJTR20T9, institute for quantum chemical exploration (IQCE), and ENEOS hydrogen trust fund. Author Notes Authors declare no competing interests.

References

1 (a) F. Atchison, P. Beaud, T. Bry´s, M. Daum, P. Fierlinger, T. Hofmann, K. Kirch, G. Kühne, G. Knopp, A. Pichlmaier, A. Serebrov, H. Spitzer, J. Wambach, J. Wambach, A. Wokaun, *Phys. Rev. B*, **2003**, 68, 094114. (b) G. Adachi, H. Sakaguchi, K. Nagao, *J. Alloys Compd.,* **1992**, *181* (1–2), 469–476. (c) R. F. Lang, J. Pienaar, E. Hogenbirk, D. Masson, R. Nolte, A. Zimbal, S. Röttger, M. L. Benabderrahmane, G. Bruno, *Nucl. Instrum. Methods Phys. Res. Sect. Accel. Spectrometers Detect. Assoc. Equip.,* **2018**, *879*, 31–38.

2 J. J. Blostein, L. A. R. Palomino, J. Dawidowski, *Phys. Rev. Lett.,* **2009**, *102*, 097401.

3 (a) T. Pirali, M. Serafini, S. Cargnin, A. A. Genazzani, *J. Med. Chem.,* **2019**, *62*, 5276–5297. (b) W. Ou, X. Xiang, R. Zou, Q. Xu, K. P. Loh, C. Su, *Angew. Chem.,* **2021**, *133*, 6427–6431.

4 (a) C. Shi, P. Fricke, L. Lin, V. Chevelkov, M. Wegstroth, K. Giller, S. Becker, M. Thanbichler, A. Lange, *Sci. Adv.,* **2015**, *1*, e1501087. (b) T. W. Marshall, *Mol. Phys.,* **1961**, *4*, 61–63.

5 (a) B. Niu, M. Niu, J. Zhang, R. Liu, H. Zhong, H. Hu, *Fuel,* **2022**, *321*, 124109. (b) L. Zhang, L. Shi, Y. Shen, Y. Miao, M. Wei, N. Qian, Y. Liu, W. Min, *Nat. Biomed. Eng.,* **2019**, *3*, 402–413. (c) L. J. Lois, T. Meng, D. Yong, J. Qiang, Z. Lei, Z. Xi, H. Younan, L. Xiaomin, *Microelectron. Reliab.,* **2022**, *135*, 114607.

6 Y. Xing, J. Cai, L. Li, M. Yang, X. Zhao, *Phys. Chem. Chem. Phys.,* **2014**, *16*, 15800–15805.

7 (a) I. Bezverkhyy, M. Giraudet, C. Dirand, M. Macaud, J.-P. J. Bellat, *J. Phys. Chem. C,* **2020**, *124*, 24756–24764. (b) R. Xiong, L. Zhang, P. Li, W. Luo, T. Tang, B. Ao, G. Sang, C. Chen, X. Yan, J. Chen, M. Hirscher, *Chem. Eng. J.,* **2020**, *391*, 123485.f

8 (a) M. Liu, L. Zhang, M. A. Little, V. Kapil, M. Ceriotti, S. Yang, L. Ding, D. L. Holden, R. Balderas-Xicohténcatl, D. He, R. Clowes, S. Y. Chong, G. Schütz, L. Chen, M. Hirscher, A. I. Cooper, *Science,* 2019, **366**, 613–620. (b) D. He, L. Zhang, T. Liu, R. Clowes, M. A. Little, M. Liu, M. Hirscher, A. I. Cooper, *Angew. Chem. Int. Ed.*, **2022**, 61, e202202450. (c) L. Zhang, S. Jee, J. Park, M. Jung, D. Wallacher, A. Franz, W. Lee, M. Yoon, K. Choi, M. Hirscher, H. Oh, *J. Am. Chem. Soc.,* **2019**, *141,* 19850–19858. (d) R. Muhammad, S. Jee, M. Jung, J. Park, S. G. Kang, K. M. Choi, H. Oh, *J. Am. Chem. Soc.,* **2021**, *143,* 8232–8236.

9 S. A. FitzGerald, C. J. Pierce, J. L. C. Rowsell, E. D. Bloch, J. A. Mason, *J. Am. Chem. Soc.,* **2013**, *135*, 9458–9464.

10 Y. Si, X. He, J. Jiang, Z. Duan, W. Wang, D. Yuan, *Nano Res.,* **2021**, *14,* 518–525.

11 L. Li, C. Ji, W. Wang, F. Wu, Y.-X. Tan, D. Yuan, *Inorg. Chem. Front.,* **2022**, *9*, 1674–1680.

12 S. A. FitzGerald, D. Mukasa, K. H. Rigdon, N. Zhang, B. R. Barnett, *J. Phys. Chem. C,* **2019**, *123*, 30427–30433.

13 F. Gao, X. Wang, W. Chen, W. Wang, W. Fan, Z. Kang, R. Wang, H. Guo, Q. Yue, D. Yuan, D. Sun, *Coord. Chem. Rev.,* **2024**, *518*, 216047.

14 H. Oh, M. Hirscher, *Eur. J. Inorg. Chem.,* **2016**, *2016*, 4278–4289.

15 J. Cai, Y. Xing, X. Zhao, *RSC Adv.,* **2012**, *2* (23), 8579.

16 L. Shere, A. K. Hill, T. J. Mays, R. Lawless, R. Brown, S. P. T. Perera, *Int. J. Hydrog. Energy,* **2024**, *55*, 319–338.

17 Abrecht, D. G.; Fultz, B. *J. Phys. Chem. C,* **2012**, *116* (42), 22245–22252.

18 K. Uchida, N. Kishimoto, S. Noro, H. Iguchi, S. Takaishi, *Dalton Trans.,* **2021**, *50* (36), 12630–12634.

19 K. Uchida, S. Tanaka, S. Adachi, H. Iguchi, R. Sakamoto, S. Takaishi, *RSC Adv.* **2024**, *14,* 11452–11455.

20 B. R. Bender, G. J. Kubas, L. H. Jones, B. I. Swanson, J. Eckert, K. B. Capps, C. D. Hoff, *J. Am. Chem. Soc.,* **1997**, *119*, 9179–9190.

21 A. J. Martínez-Martínez, N. H. Rees, A. S. Weller, *Angew. Chem. Int. Ed.,* **2019**, *58,* 16873–16877.

22 I. Weinrauch, I. Savchenko, D. Denysenko, S. M. Souliou, H.-H. Kim, M. Le Tacon, L. L. Daemen, Y. Cheng, A. Mavrandonakis, A. J. Ramirez-Cuesta, D. Volkmer, G. Schütz, M. Hirscher, T. Heine, *Nat. Commun.,* **2017**, *8*, 14496.

23 N. F. Cessford, N. A. Seaton, T. Düren, *Ind. Eng. Chem. Res.,* **2012**, *51*, 4911–4921.

24 S. A. FitzGerald, C. J. Pierce, J. L. C. Rowsell, E. D. Bloch, J. A. Mason, *J. Am. Chem. Soc.,* **2013**, *135*, 9458–9464.

25 C. M. Simon, B. Smit, M. Haranczyk, *Comput. Phys. Commun.,* **2016**, *200*, 364–380.

26 R. K. Upmacis, M. Poliakoff, J. J. Turner, *J. Am. Chem. Soc.,* **1986**, *108*, 3645–3651.

27 W. A. King, X.-L. Luo, B. L. Scott, G. J. Kubas, K. W. Zilm, *J. Am. Chem. Soc.,* **1996**, *118*, 6782–6783.

28 Gaussian 16, Revision C.01, M. J. Frisch, G. W. Trucks, H. B. Schlegel, G. E. Scuseria, M. A. Robb, J. R. Cheeseman, G. Scalmani, V. Barone, G. A. Petersson, H. Nakatsuji, X. Li, M. Caricato, A. V. Marenich, J. Bloino, B. G. Janesko, R. Gomperts, B. Mennucci, H. P. Hratchian, J. V. Ortiz, A. F. Izmaylov, J. L. Sonnenberg, D. Williams-Young, F. Ding, F. Lipparini, F. Egidi, J. Goings, B. Peng, A. Petrone, T. Henderson, D. Ranasinghe, V. G. Zakrzewski, J. Gao, N. Rega, G. Zheng, W. Liang, M. Hada, M. Ehara, K. Toyota, R. Fukuda, J. Hasegawa, M. Ishida, T. Nakajima, Y. Honda, O. Kitao, H. Nakai, T. Vreven, K. Throssell, J. A. Montgomery, Jr., J. E. Peralta, F. Ogliaro, M. J. Bearpark, J. J. Heyd, E. N. Brothers, K. N. Kudin, V. N. Staroverov, T. A. Keith, R. Kobayashi, J. Normand, K. Raghavachari, A. P. Rendell, J. C. Burant, S. S. Iyengar, J. Tomasi, M. Cossi, J. M. Millam, M. Klene, C. Adamo, R. Cammi, J. W. Ochterski, R. L. Martin, K. Morokuma, O. Farkas, J. B. Foresman, and D. J. Fox, Gaussian, Inc., Wallingford CT, **2016**.

29 (a) D. A. Becke, *J. Chem. Phys.,* **1993**, *98* (7), 5648–5652. (b) C. Lee, W. Yang, R. G. Parr, *Phys. Rev. B,* **1988**, *37*, 785–789.

30 Y. Zhao, D. G. Truhlar, *Theor. Chem. Acc.,* **2008**, *120*, 215–241.

31 J.-D. Chai, M. Head-Gordon, *Phys. Chem. Chem. Phys.,* **2008**, *10* (44), 6615.

32 F. Weigend, R. Ahlrichs, *Phys. Chem. Chem. Phys.,* **2005**, *7*.

33 (a) E. R. Davidson, *Chem. Phys. Lett.,* **1996**, *260*, 514–518. (b) T. H. Dunning, *J. Chem. Phys.,* **1989**, *90*, 1007–1023.

34 (a) V. A. Rassolov, J. A. Pople, M. A. Ratner, T. L. Windus, *J. Chem. Phys.,* **1998**, *109* (4), 1223–1229. (b) V. A. Rassolov, M. A. Ratner, J. A. Pople, P. C. Redfern, L. A. Curtiss, *J. Comput. Chem.,* **2001**, *22* (9), 976–984. (c) P. C. Hariharan, J. A. Pople, *Mol. Phys.,* **1974**, *27* (1), 209–214. (d) R. C. Binning, L. A. Curtiss, *J. Comput. Chem.,* **1990**, *11* (10), 1206–1216. (e) J.-P. Blaudeau, M. P. McGrath, L. A. Curtiss, L. Radom, *J. Chem. Phys.,* **1997**, *107* (13), 5016–5021. (f) M. M. Francl, W. J. Pietro, W. J. Hehre, J. S. Binkley, M. S. Gordon, D. J. DeFrees, J. A. Pople, *J. Chem. Phys.,* **1982**, *77* (7), 3654–3665. (g) R. Ditchfield, W. J. Hehre, J. A. Pople, *J. Chem. Phys.,* **1971**, *54* (2), 724–728. (h) W. J. Hehre, R. Ditchfield, J. Pople, *J. Chem. Phys.,* **1972**, *56* (5), 2257–2261. (i) P. C. Hariharan, J. A. Pople, *Theor. Chim. Acta,* **1973**, *28* (3), 213–222.

35 W. A. King, B. L. Scott, J. Eckert, G. J. Kubas, *Inorg. Chem.,* **1999**, *38* (6), 1069–1084.

Data availability

All data associated with this manuscript are available in the ESI. The adsorption isotherms data is format of origin software (.opju)